Carbon 102 (2016) 1–9

Contents lists available at ScienceDirect

Carbon

journal homepage: www.elsevier.com/locate/carbon

Vapor–solid preparation of densely distributed and small-sized graphene nanoflakes on one-dimensional nanomaterials for low-field and highly stable field emission

Jian-Hua Deng [a, *], Li-Na Deng [a], Rui-Nan Liu [a], A-Long Han [a], De-Jun Li [a], Guo-An Cheng [b]

[a] College of Physics and Materials Science, Tianjin Normal University, Tianjin, 300387, China
[b] Key Laboratory of Beam Technology and Material Modification of Ministry of Education, Beijing Normal University, Beijing, 100875, China

ARTICLE INFO

Article history:
Received 27 December 2015
Received in revised form
2 February 2016
Accepted 8 February 2016
Available online 11 February 2016

ABSTRACT

Differently shaped two-dimensional (2-D) graphene nanoflakes (GNFs) were prepared on one-dimensional (1-D) carbon nanotubes (CNTs) and silicon nanowires (SiNWs) forming 2-D–1-D composites by using microwave plasma enhanced chemical vapor deposition. The GNFs are vertically aligned on 1-D nanomaterials with their sharp edges (less than 10 layers) unfolded outside and are rich in defects. GNF–CNT (or SiNW) composites with densely distributed and small-sized GNFs and not obviously thickened CNTs (or SiNWs) are found to have superior FE properties. The optimal FE performance obtained from the GNF–CNT composites shows a low threshold field of 1.54 V/μm and an extremely large maximum emission current density of 75.46 mA/cm^2, far better than 1.77 V/μm and 27.90 mA/cm^2 for the pristine CNTs, respectively. The FE improvement is ascribed to the significant increase of active emission sites and also the preservation of the high aspect ratio of CNTs. Furthermore, longtime (30 h) stable FE is achieved from GNF–CNT composites with optimal shapes at a high mean emission current density of 45.47 mA/cm^2 and a low operation field of 1.766 V/μm, showing promising prospects in high-performance vacuum electronic device applications.

© 2016 Elsevier Ltd. All rights reserved.

1. Introduction

Graphene is a two-dimensional (2-D) honeycomb C network having fascinating electrical, mechanical, and optical properties, and it has aroused intensive interest in a wide range of novel applications over the past few years [1–4]. With the great progress in research on mono- and bi-layer graphene, recent attention is being paid on its multilayer counterparts due to their characteristics of low cost and easy preparation. Multilayer graphenes have been demonstrated great potentials in various applications such as field-effect transistors [5], photo detectors [6], energy storage [7], and so on. Graphene has also been considered as an excellent field emission (FE) cathode material due to its superior conductivity, chemical inertness, and unique 2-D structure [8–11]. High-efficiency FE is highly expected in device applications such as displays (liquid crystal and flat panel displays), lighting lamps, and X-ray tubes. FE is a quantum mechanical tunneling phenomenon under high applied fields which are of the order of 10^9 V/m [12]. Easy electron tunneling requires emitters having high aspect ratio, nanosharp tip, and low work function. In this regard, one-dimensional (1-D) nanomaterials such as carbon nanotubes (CNTs) [13,14], silicon nanowires (SiNWs) [15], TiO_2 nanotubes [16], and ZnO nanowires [17,18] are good candidates and their FE performance has been intensively studied in the last few decades. However, FE is believed to predominantly occur from their tips rather than the side walls due to the fact that local applied fields at emission sites large enough for electron tunneling can only be concentrated at the tips [19]. A report from Nakayama et al. indicates that the local applied field at a CNT tip is 2.8 times higher than its side walls [20]. Improved FE properties can thus be desired from 1-D nanomaterials by adding new active emission sites to their side walls. Graphene with nanosharp edges is considered as a good candidate and many attempts have recently been made to obtain graphene–1-D nanomaterial composites or hybrids, such as vertical ZnO nanowire–graphene hybrids [21–23], graphene–metallic nanowire hybrids [24], and graphene–CNT composites [25,26]. However, the graphene in all of these hybrids or composites is flat-lying and merely used as a substrate and the FE enhancement from its

* Corresponding author.
E-mail address: jhdeng1983@163.com (J.-H. Deng).

http://dx.doi.org/10.1016/j.carbon.2016.02.026
0008-6223/© 2016 Elsevier Ltd. All rights reserved.

edge is not exploited. Preparing vertical graphenes on 1-D nanomaterials is thus highly desired. SiNWs and CNTs have been used as substrates to prepare vertical graphenes and enhanced FE performance from these composites has also been reported [27–29]. We have prepared few-layer graphene–CNT composites by using radio frequency sputtering deposition and obtained highly improved FE performance as compared with that of pure few-layer graphene or CNT arrays [30,31]. However, these composites are found to have poor FE stability at high FE currents (FE current drops more than 15% in 5 h). In comparison with CNTs, graphene-based emitters have better FE stability due to the fact that the unique 2-D area of graphene facilitates heat dispersion and weakens Joule heating induced decrease of active emission sites [32–34]. The composites we prepared only have extremely sparsely distributed graphene [30,31], thus the contribution to FE stability from the graphene is not obvious. Besides growing graphene, coating CNTs is also an effective approach widely used to improve the FE stability of CNT emitters. For example, ZnO nanoparticles [35], Ru nanoparticles [36], and amorphous C [37,38] have been used to coating CNTs and improve their FE stability.

In the present study, differently shaped graphene nanoflakes (GNFs) were grown on CNTs and SiNWs without a catalyst by using microwave plasma enhanced chemical vapor deposition (PECVD), and the FE performance of those 2-D–1-D composites is investigated. They are found to have far better FE capability and stability than the bare CNTs or SiNWs and in particular, composites with densely distributed and small-sized GNFs and not obviously thickened CNTs are found to have superior FE performance to that of those with sparsely distributed and large-sized GNFs and considerably thickened CNTs. Together with the excellent FE stability, our 2-D–1-D composites with optimal shapes may find applications calling for high current, low operation voltage, and longtime stable FE.

2. Experimental details

2.1. Preparation of CNTs and SiNWs

The preparation of GNF–CNT composites is schematically shown in Fig. 1a. It follows a process of growing CNTs on n-(100) Si wafers by using thermal CVD and growing GNFs on the as-received CNTs by using microwave PECVD. The Si wafers were first bombarded by iron ions using a metal vapor vacuum arc ion source at 10 kV for 15 min to improve the adhesion of CNTs to Si wafers [39]. Then an iron film of ~5 nm in thickness was deposited on the Si wafers as a catalyst by using magnetron sputtering. The Si wafers (~2 × 2 cm^2) were then placed in a tubular furnace for the CNT growth. We first processed the catalyst under 400 sccm H_2 at 580 °C for 1 h and 150 sccm NH_3 at 750 °C for 10 min to promote its activity. The growth of CNTs was carried out under 600 sccm H_2 and 87 sccm C_2H_2 at 750 °C for 30 min. The thus-prepared CNTs are ~20 μm in length, as shown in Fig. S1a. The preparation of SiNWs was performed on n-Si (100) wafers using Ag as an etching catalyst [40]. Cleaned Si wafers (~2 × 2 cm^2 in area) were first immersed into a HF–$AgNO_3$ solution ($AgNO_3$:HF:H_2O = 2:10:38, vol%) for 1 min to deposit the Ag catalyst and then transferred to a HF–H_2O_2 solution (H_2O_2:HF:H_2O = 1:10:39, vol%) for 45 min to electrolessly prepare SiNWs. The concentration for $AgNO_3$, HF, and H_2O_2 are 0.01, 4, and 0.176 mol/L, respectively. The as-received SiNWs are ~17 μm in length, as shown in Fig. S1b.

2.2. Preparation of GNFs

Fig. 1b shows a schematic of the PECVD setup used for the growth of GNFs on the as-received CNTs and SiNWs. The distance between the samples and plasma flame was ~1 cm. The growth of GNFs was carried out in a C_2H_2/H_2 gas mixture at 1 kPa and 800 °C for 4 h. The GNF shape was controlled by tuning the C_2H_2/H_2 gas ratios and microwave powers. The GNF–CNT composites were further annealed at 1050 °C for 2.5 h to improve the adhesion of CNTs to substrates [39].

2.3. Structural characterizations

The surface morphology of the samples was characterized using a scanning electron microscope (SEM, S–4800, Hitachi, Japan) operated at 10 kV, and their fine structure was observed using a transmission electron microscope (TEM, JEM–2010, JEOL, Japan) under 200 kV. The samples were first ultrasonicated (50 W) in an ultrasonic bath for 15 min and then the resultant solution was dropped onto a copper grid and air-dry before being observed by the TEM. A Raman spectrometer (LabRAM Aramis, Horiba Jobin Yvon, France) operating with a 633 nm He–Ne laser as the excitation source was employed to perform the defect analysis and qualitatively characterize the crystallinity of GNFs. A photoelectron spectrometer (AC–2, Riken Keiki, Japan, spot area: 4 × 4 mm^2) operated in the atmosphere was used to characterize the work function of our samples.

2.4. FE measurements

The FE properties of the samples were estimated by a classical parallel diode setup in an ultrahigh vacuum chamber (~1.0 × 10^{-7} Pa), as schematically shown in Fig. 1c. The samples (~2 × 2 mm^2) were used as the cathode against a stainless steel plate as the anode. A tunable DC bias voltage (0–10 kV) was applied

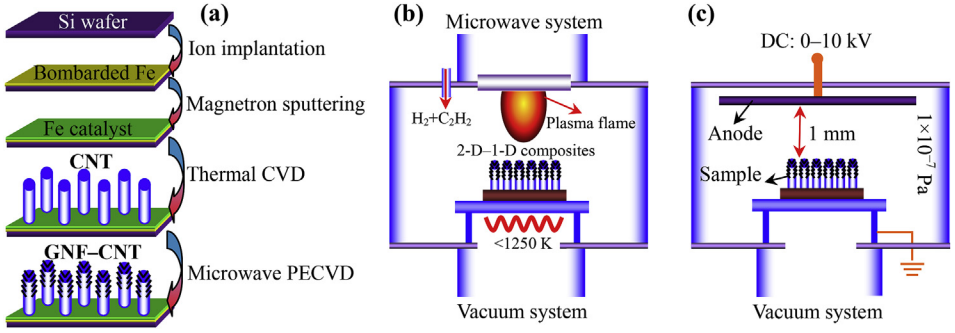

Fig. 1. (a) Schematic of the preparation of GNF–CNT composites. (b) The microwave PECVD setup used for the growth of GNFs on CNTs and SiNWs. (c) The diode-type setup used for FE tests. (A colour version of this figure can be viewed online.)

on the anode during FE tests while grounding the cathode. In order to reduce the bias voltage on the anode, the cathode–anode gap was set as 1 mm for testing the CNT-based samples and 500 μm for testing the SiNW-based ones. The FE results were recorded by a computer in terms of emission current (*I*) *versus* applied voltage (*V*). The applied field (*E*) was calculated by dividing the *V* with the anode–cathode gap and the emission current density (*J*) was obtained by dividing the *I* with the sample areas.

3. Results and discussion

3.1. Structural characterization of differently shaped GNF–CNT composites

The key growth parameter used to control the morphology of GNFs was the C_2H_2 gas flows (2, 4, 6, 8, and 10 sccm), and the others were 1 kPa, 150 W, 800 °C, 10 sccm H_2, and 4 h Fig. 2 shows typical top-view SEM images of pristine CNTs and differently shaped GNF–CNT composites, and the insets are the corresponding side-view SEM images. The pristine CNTs are 30–60 nm in diameter with randomly distributed tips and smooth surfaces. For the 2 sccm sample, GNFs less than 60 nm in width are sparsely grown on CNTs and the thickening of CNTs is not obvious. For the 4 sccm sample, the GNFs are less than 100 nm in width with their sharp edges unfolded outside and the diameter of CNTs increases slightly. Upon the 6, 8, and 10 sccm samples, the GNF size gradually decreases and the CNT diameter increases significantly. These results indicate the distribution density and size of GNFs and the thickening of CNTs could be readily controlled by adjusting the C concentrations. Generally, low C concentration corresponds with the growth of sparsely distributed and small-sized GNFs and the thickening of CNTs is not obvious (see Fig. 2b), while high C concentrations are associated with the growth of densely distributed and small-sized GNFs and also the considerable thickening of CNTs (see Fig. 2e and f).

The fine structure of our samples was further characterized by using a TEM. Fig. 3a–d shows high-resolution TEM images of pristine CNTs and GNF–CNT composites prepared under 2, 4, and 6 sccm C_2H_2, respectively, and the insets are the corresponding low-resolution TEM images. The CNT has a hollow core and more than 60 parallel graphite walls and a tip of ~90 nm in diameter (inset of Fig. 3a). The CNT of the 2 sccm sample is covered by sparsely distributed and small-sized GNFs and its capped tip is removed by the hydrogen plasma, with an open end left (inset of Fig. 3b). The consistent atom arrangement between the GNF and the CNT indicates that the growth of GNF is self-assembled. A thin GNF edge of ~6 layers is observed from the 4 sccm sample and the surface of GNF is defected. Upon the 6 sccm sample, a large amount of GNFs are found to be shaken off from the CNTs, leaving CNTs with sharp-edged asperities (inset of Fig. 3d), suggesting a poor adhesion of the GNFs to CNTs in this condition. We ascribe this phenomenon to the quick deposition of C atoms. The vapor–solid growth of vertical graphenes have been well addressed previously [30,41–43]. In brief, activated C atoms deposit on CNTs and nucleate at defects. They diffuse on the surface of graphenes under the help of plasma electric field and form covalent bonds at the edges before being re-evaporated, resulting in the 2-D growth of graphenes. In the case of high C concentrations, large-amount activated C atoms quickly deposit on CNTs and the atom–atom collision greatly limits their diffusion, resulting in that plenty of C atoms are loosely bonded on the surface of CNTs by means of forming a defect-rich C layer rather than nucleating for the growth of GNFs. The defects in this C layer can also serve as nucleation sites for growing new GNFs, and these newly grown GNFs as well as the loosely bonded C layer are easy to be shaken off from the CNTs during the preparation of TEM samples. Pure GNFs were prepared on Si wafers under the same growth conditions for TEM observations and Raman analyses. The top-view SEM images of the pure GNFs are shown in Fig. S2. It can be seen that all the GNFs prepared on Si wafers have lower distribution densities than those prepared on CNTs due to the low density of intrinsic defects on Si wafers [30,43]. Fig. 3e shows the low-resolution TEM image of the 4 sccm pure GNFs. The GNFs are ~400 nm in width (inset of Fig. 3e) and have almost transparent edges, suggesting that the GNFs are thin graphenes. This thin

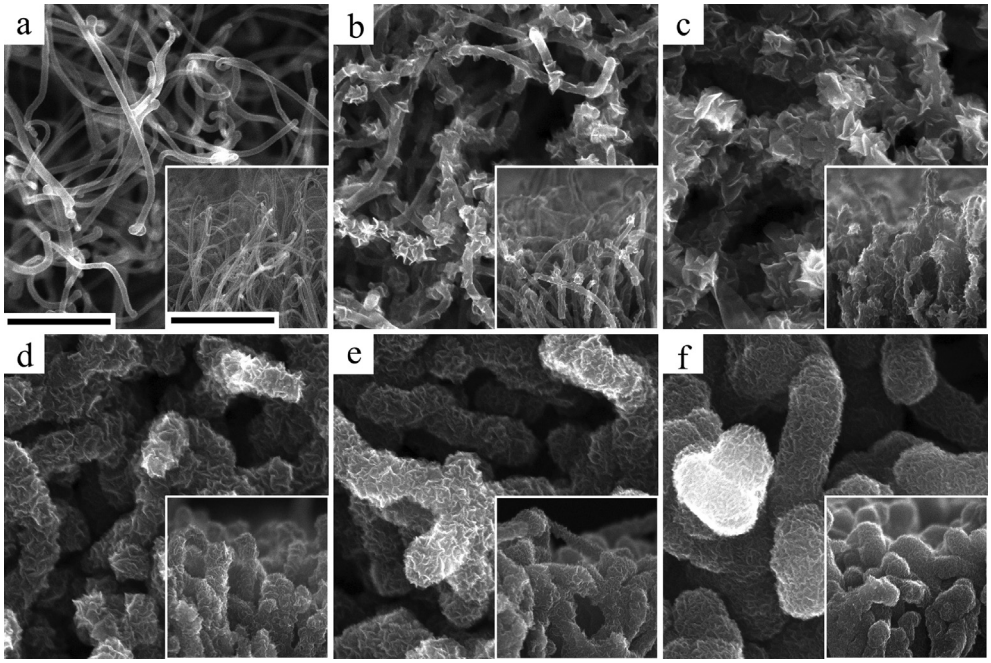

Fig. 2. Top-view SEM images of (a) pristine CNTs and GNF–CNT composites synthesized under (b) 2, (c) 4, (d) 6, (e) 8, and (f) 10 sccm C_2H_2. The insets are the corresponding side-view SEM images. Other growth conditions are 1 kPa, 150 W, 800 °C, 10 sccm H_2, and 4 h. The scale bars in (a–f) are 500 nm and in the insets of (a–f) are 1 μm.

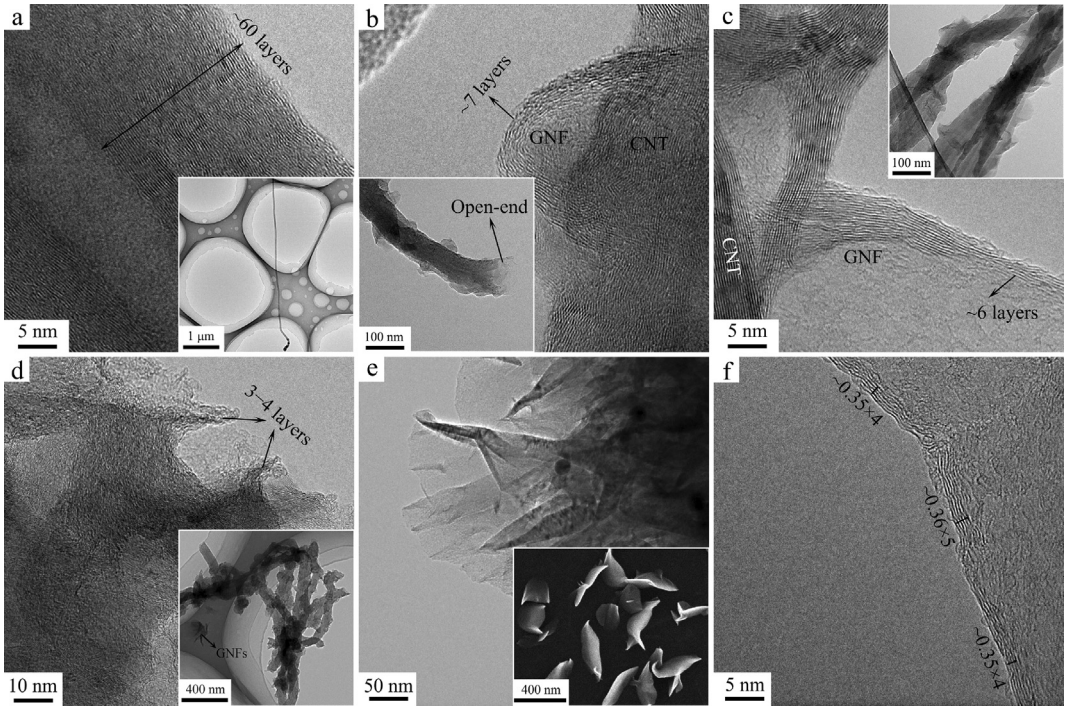

Fig. 3. High-resolution TEM images of (a) pristine CNTs and GNF–CNT composites prepared under (b) 2, (c) 4, and (d) 6 sccm C_2H_2. Insets are the corresponding low-resolution TEM images. (e) Low- and (f) high-resolution TEM images of pure GNFs prepared on Si wafers under 4 sccm C_2H_2. Inset of (e) is the corresponding top-view SEM image.

nature of GNFs can also be clearly seen from the GNF of 4–5 layers shown in Fig. 3f. The interlayer spacing of GNFs is larger than 0.34 nm for typical bulk graphite due to the reduction of the van der Waals interaction.

Raman spectroscopy is a widely used non-destructive tool to obtain structural information from carbonaceous materials [44–46]. The intensity ratio of the D (~1330 cm^{-1}) and G (~1583 cm^{-1}) peaks (I_D/I_G) could be used to evaluate the perfection of carbonaceous materials, and the intensity ratio of the Raman 2D (~1330 cm^{-1}) and G peaks (I_{2D}/I_G) could be used to roughly calculate the layer of graphene [46]. For example, the I_{2D}/I_G value for mono-layer graphenes is ~4 [46] and for few-layer (less than 10 layers) graphenes is usually larger than 1.0 [30,47]. However, it should be noted that the penetration depth of the 633 nm Raman laser in carbonaceous materials could reach hundreds of nanometers, which are larger than the size of GNFs (usually less than 100 nm). Thus, the Raman spectroscopy from our GNF–CNT composites would bring information from both the GNFs and the underlying CNTs especially for composites with sparsely distributed GNFs (correspond with the 2 and 4 sccm samples shown in Fig. 2b and c). As an example, the GNFs from the 2 sccm sample have been clearly demonstrated to be less than 10 layers (Fig. 3b), which should have a I_{2D}/I_G ratio larger than 1.0 [30,47], but the actual I_{2D}/I_G ratio for this GNF–CNT sample is only ~0.38 (Fig. S3) due to the influence of the underlying CNTs. In order to eliminate the influence from CNTs, Raman characterization was only performed on pure GNFs prepared under the same growth conditions (see Fig. S2), as shown in Fig. 4. The large I_D/I_G values (1.92–2.53, inset of Fig. 4) indicate that the GNFs are rich in defects. The GNFs prepared under 2, 4, and 6 sccm C_2H_2 have I_{2D}/I_G values larger than 1.0, indicating that these GNFs are ultrathin graphenes, in good agreement with our TEM observations. The small I_{2D}/I_G value (~0.54) for the 10 sccm GNFs indicates that they are thick C flakes. This can also be clearly seen from the GNF edge with more than 10 layers shown in Fig. S4. The above TEM and Raman results indicate

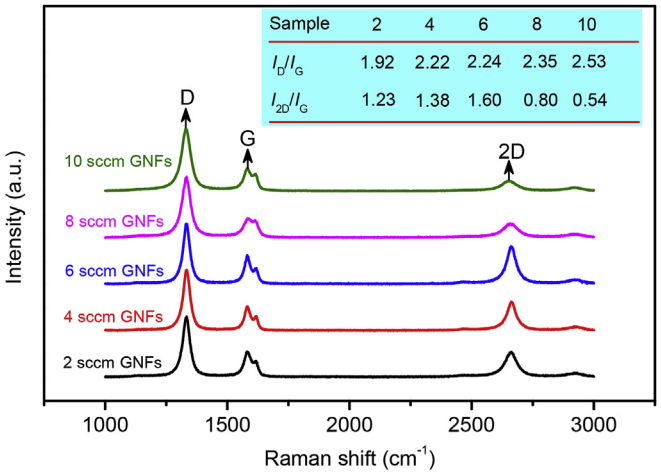

Fig. 4. Raman spectra of pure GNFs prepared under 2, 4, 6, 8, and 10 sccm C_2H_2. I_D, I_G, and I_{2D} are the intensities of the D, G, and 2D peaks, respectively. (A colour version of this figure can be viewed online.)

that the thickness of GNFs is also dependent on the C concentrations. Preparing GNFs under a very high C concentration not only leads to the significant increase of CNT diameters (see Fig. 2f) but also leads to the increase of graphene layers (Fig. S4).

3.2. FE properties of GNF–CNT composites

The FE performance of pristine CNTs and differently shaped GNF–CNT composites was measured for comparison. The *J–E* (*J versus E*, Fig. 5a) performance is used to evaluate the FE capability of the samples and the corresponding FE results are shown in Table 1. Emitters with high FE capability are associated with low turn-on (E_{on}, *E* at 10 μA/cm^2) and threshold fields (E_{th}, *E* at 10 mA/cm^2)

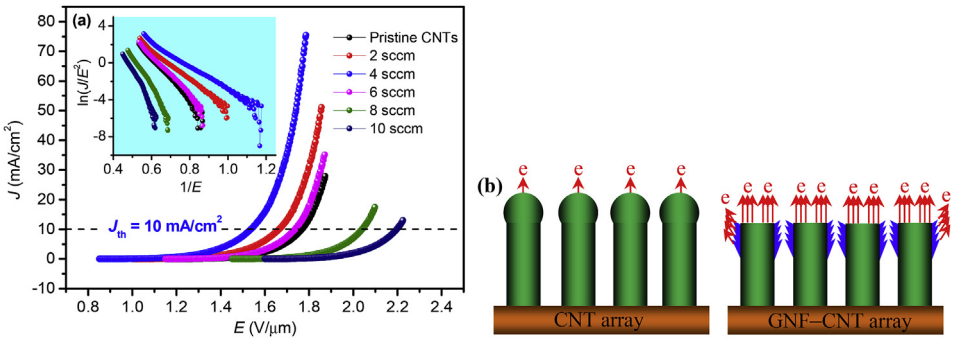

Fig. 5. (a) FE J–E curves of pristine CNTs and GNF–CNT composites prepared under 2, 4, 6, 8, and 10 sccm C_2H_2. Inset exhibits the corresponding F–N plots. (b) Schematics of the FE from pristine CNTs and GNF–CNT composites. The "e" represents emitting electrons. (A colour version of this figure can be viewed online.)

Table 1
FE results of pristine CNTs and GNF–CNT composites prepared under 2, 4, 6, 8, and 10 sccm C_2H_2.

Sample	E_{on} (V/μm)	E_{th} (V/μm)	J_{max} (mA/cm^2)	φ (eV)	β
CNTs	1.20	1.77	27.90	4.91	3447
2 sccm	1.02	1.66	51.13	4.75	4330
4 sccm	0.87	1.54	75.46	4.72	5218
6 sccm	1.16	1.74	35.08	4.64	3356
8 sccm	1.49	2.04	17.47	4.68	2454
10 sccm	1.62	2.20	13.02	4.65	2147

and large maximum emission current density (J_{max}). Optimal FE response is obtained from the 4 sccm sample, with an ultralow E_{on} of 0.87 V/μm and E_{th} of 1.54 V/μm and an extremely large J_{max} of 75.46 mA/cm^2, which are far better than the 1.20 and 1.77 V/μm and 27.90 mA/cm^2 for the pristine CNTs, respectively. These results from the 4 sccm sample are comparable or even better than a great many recently well-verified superior emitters such as single layer graphenes (E_{on}: 2.30 V/μm; E_{th}: 5.20 V/μm) [8], TiO_2 nanotubes (E_{on}: 17.20 V/μm) [16], hierarchical ZnO/Si nanotrees (E_{on}: 2.18 V/μm) [18], as-grown few-walled CNTs (E_{on}: 2.53 V/μm) [48], and vertical aligned few-layer graphene sheets (E_{on}: 1.80 V/μm) [49]. For the 6, 8, and 10 sccm samples, the FE *J–E* curves gradually shift to the high-*E* region, indicating their gradually deteriorated FE capability. The poorest FE performance is obtained from the 10 sccm sample, with a high E_{on} of 1.62 V/μm and E_{th} of 2.20 V/μm and a small J_{max} of 13.02 mA/cm^2. Fowler–Nordheim (*F–N*) theory is used to analyze the FE performance of emitters [50]. The inset of Fig. 5a shows the *F–N* plots, presented in terms of $\ln(J/E^2)$ *versus* $1/E$. An approximate linearity behavior is observed in the high–*E* regions of the *F–N* plots, indicating that the electrons are mainly extracted through quantum tunneling in this regime [50]. The field enhancement factor (β) is a parameter closely related to the aspect ratio, the radius of curvature, and the number density of active emission sites of emitters. It is obtained on the basis of the following *F–N* equation:

$$J = A\left(\frac{\beta^2 E^2}{\phi}\right)\exp\left(-\frac{B\phi^{3/2}}{\beta E}\right) \quad (1)$$

where the A and B are constants of 1.54×10^{-6} A eV V^{-2} and 6.83×10^3 eV$^{-3/2}$ V μm^{-1}, respectively. The work function (φ), which demonstrates the energy difference between the Fermi level of emitters and the vacuum level, is determined by using a photoelectron spectrometer. The φ values for the GNF–CNT composites (4.64–4.75 eV) are smaller than 4.91 eV for the pristine CNTs. This is attributed to the increased state density of defects induced rising of Fermi Level after the growth of GNFs under plasma [51]. The β is calculated from the slope of the high–*E* region of *F–N* plots using the following equation:

$$\beta = -\frac{B\phi^{3/2}}{\text{slope}} \quad (2)$$

It can be seen from Table 1 that the change of β is dramatic, and the variation trend of FE capability is in great agreement with that of the β. As an example, GNF–CNT composites with the best and the worst FE performance are found to have the largest (~5218) and the smallest (~2147) β values, respectively. In comparison with the small change of the work function (from 4.67 to 4.75 eV), this considerable change of the field enhancement factor (from 2147 to 5218) indicates that the FE capability of our emitters is β-rather than φ-dependent. Fig. 5b schematically illustrates the FE from pristine CNTs and GNF–CNT composites. For pristine CNTs, FE mainly occurs from their thick tips (~90 nm in diameter, inset of Fig. 3a) and the smooth tube walls remain less sensitive to FE [19]. Upon GNF–CNT composites, the open end of CNTs [52,53], the densely distributed and sharp-edged GNFs [8], the wrinkles on GNFs [54], and the defects created by hydrogen plasma [51,55,56], all of them can play as highly efficient emission sites during FE and thereby leading to their superior FE performance. The gradually deteriorated FE response for the 6, 8, and 10 sccm samples is mainly ascribed to the increase of CNT diameters that lowers their aspect ratios.

The FE stability (*J versus* time) of pristine CNTs and GNF–CNT composites with typical morphology (the 4 and 8 sccm samples) was evaluated. Fig. 6a shows their short-term (5 min) FE stability at the maximum applied fields (E_{max}, corresponding with the maximum *E* of the FE *J–E* curves shown in Fig. 5), with the emission current recorded in every 5 s. For pristine CNTs, the *J* decreases sharply and then a vacuum breakdown event is initiated [34,39,57], which is absent for the GNF–CNT composites. We employ a parameter, J_{drop}, to characterize the FE stability of the samples. It is calculated from $(J_{first} - J_{last})/J_{first}$, where J_{first} and J_{last} are the first and the last recorded *J* in a test, respectively. The J_{drop} values of the 4 and 8 sccm samples are 24.3% and 25.1%, respectively, and continuous current falling is observed for both types of samples. This significant deterioration of the FE performance is mainly ascribed to the Joule heating induced decrease of active emission sites considering the *J* is more than 50 mA/cm^2 [32–34]. This continuous electron emission is a so-called aging process and is believed to be beneficial for improving the FE stability of emitters [58–60]. Fig. 6b shows the FE stability of the samples at $E = E_{max} - 0.01$. No current breakdown was observed for all the samples in this condition. The J_{drop} values for the pristine CNTs and the 4 and 8 sccm GNF–CNT composites are 30.5%, 17.0%, and 17.2%, respectively, indicating that the growth

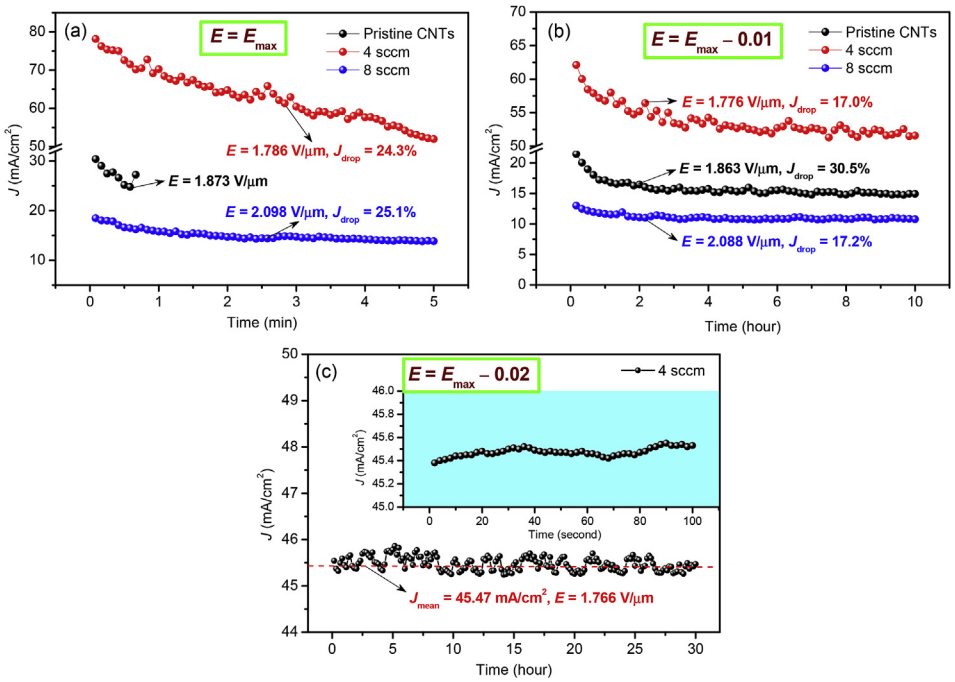

Fig. 6. FE stability of pristine CNTs and GNF–CNT composites prepared under 4 and 8 sccm C_2H_2. (a) 5 min FE stability at $E = E_{max}$. (b) 10 h FE stability at $E = E_{max} - 0.01$. (c) 30 h FE stability of the 4 sccm sample at $E = E_{max} - 0.02$. The inset is the 100 s FE stability of the same sample at $E = E_{max} - 0.02$, with the testing data recorded in every 2 s. (A colour version of this figure can be viewed online.)

of GNFs greatly improves the FE stability of our emitters. The FE stability at $E = E_{max} - 0.01$ is found to be better than that at $E = E_{max}$ for same types of samples. It is expected that the lifetime of a FE device can be extended by being pre-aged at a higher E and than working at a lower E. In this regard, 30 h FE stability of the same 4 sccm sample at $E = E_{max} - 0.02$ was further tested right after the 10 h test at $E = E_{max} - 0.01$, as shown in Fig. 6c. The FE current is quite stable at a low constant E of 1.776 V/μm, with little current fluctuations (see the inset of Fig. 6c, presented with the FE data recorded in every 2 s) and a high mean emission current density (J_{mean}) up to 45.47 mA/cm^2.

3.3. Influence of GNF size on the FE performance of GNF–CNT composites

The size of GNFs also plays a key role in the FE performance of GNF–CNT composites. We decreased the microwave power from 150 to 100 W to prepare GNF–CNT composites with large-sized GNFs (other growth parameters are 1 kPa, 800 °C, 4 sccm C_2H_2, 10 sccm H_2, and 4 h), as shown in Fig. 7a. The GNFs is ~500 nm in width with their sharp edges unfolded outside forming a flower-like appearance (inset of Fig. 7a), far larger than ~100 nm of the 150 W sample (Fig. 2c). The space among adjacent CNTs disappears due to the dense distribution of large-sized GNFs. Fig. 7b shows the FE J–E performance of the 100 W (large-sized GNFs, Fig. 7a) and the 150 W (small-sized GNFs, Fig. 2c) samples. It can be seen that the 100 W sample has far poorer FE performance than that of the 150 W one, with a high E_{th} of 1.95 V/μm and a small J_{max} of 26.56 mA/cm^2. We ascribe this FE deterioration to the highly increased field screening due to the growth of large-sized GNFs that shields the field enhancement from the high-aspect-ratio CNTs [61,62]. The above results indicate that both the densely distributed and small-sized GNFs with nanosharp edges, which provide numerous protrusions as active emission sites, and the CNTs with high aspect ratios, which facilitate electron tunneling through barriers, are responsible for the superior FE performance of our GNF–CNT composites.

3.4. FE performance of GNF–SiNW composites

Differently shaped GNFs were also prepared on SiNWs to support the above findings. Fig. 8a–d shows side-view SEM images of pristine SiNWs and GNF–SiNW composites prepared under 4, 5, and 6 sccm C_2H_2, respectively. The other growth conditions were 1 kPa, 150 W, 800 °C, 10 sccm H_2, and 4 h. The pristine SiNWs are well aligned with diameters less than 100 nm and defected surfaces (Fig. 8a). The GNFs of the 4 sccm sample are ~100 nm in width and densely distributed on SiNWs (Fig. 8b). The size of GNFs for the 5 and 6 sccm samples is slightly smaller and in particular, the diameter of SiNWs increases significantly and the space among adjacent SiNWs gradually disappears (Fig. 8c and d). Fig. 8e shows a low-resolution TEM image of the 4 sccm sample. It can be seen that the GNFs are densely grown on SiNWs and the almost transparent unfolded part indicates that the GNFs are thin graphenes. The thin edge of 3–5 layers shown in Fig. 8f and the large Raman I_{2D}/I_G ratio of ~1.16 shown in Fig. S5 also demonstrate the thin nature of our GNFs [46].

Fig. 9a shows FE J–E curves of the pristine SiNWs and GNF–SiNW composites prepared under 4, 5, and 6 sccm C_2H_2. The E at 1 mA/cm^2 is as high as 7.08 V/μm and the J_{max} is only 1.18 mA/cm^2 for the pristine SiNWs, while those for the 4 sccm sample are 3.37 V/μm and 3.54 mA/cm^2, respectively. This great FE improvement is mainly ascribed to the growth of sharp-edged GNFs that provides plenty of highly efficient emission sites. In comparison with the 4 sccm sample, the FE performance of the 5 and 6 sccm samples deteriorates dramatically. The E at 1 mA/cm^2 (6.40 V/μm) and the J_{max} (1.24 mA/cm^2) of the 6 sccm sample even approach those of the pristine SiNWs. This FE deterioration is ascribed to the significant increase of the SiNW diameters that lowers the local applied fields at emission sites. Comparison of the FE performance

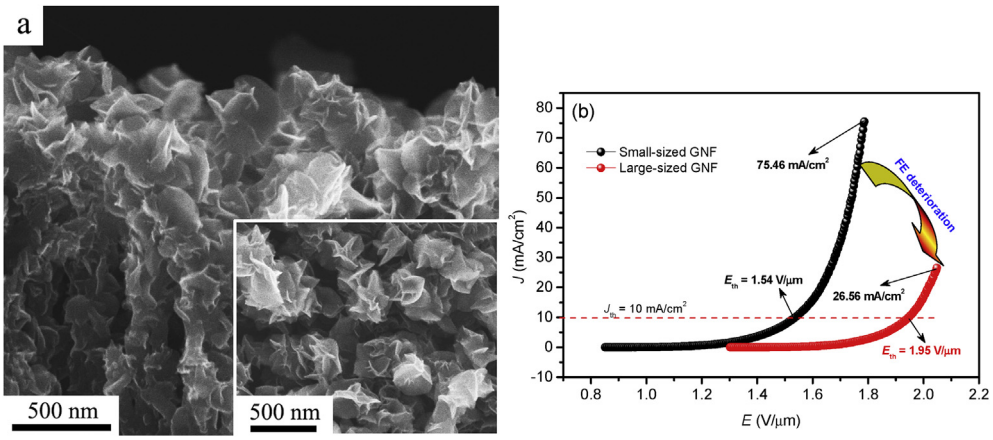

Fig. 7. (a) Side- and (Inset) top-view SEM images of large-sized GNFs grown on CNTs. Growth conditions are 1 kPa, 100 W, 800 °C, 4 sccm C_2H_2, 10 sccm H_2, and 4 h (b) FE *J*–*E* curves of GNF–CNT composites with small- and large-sized GNFs. (A colour version of this figure can be viewed online.)

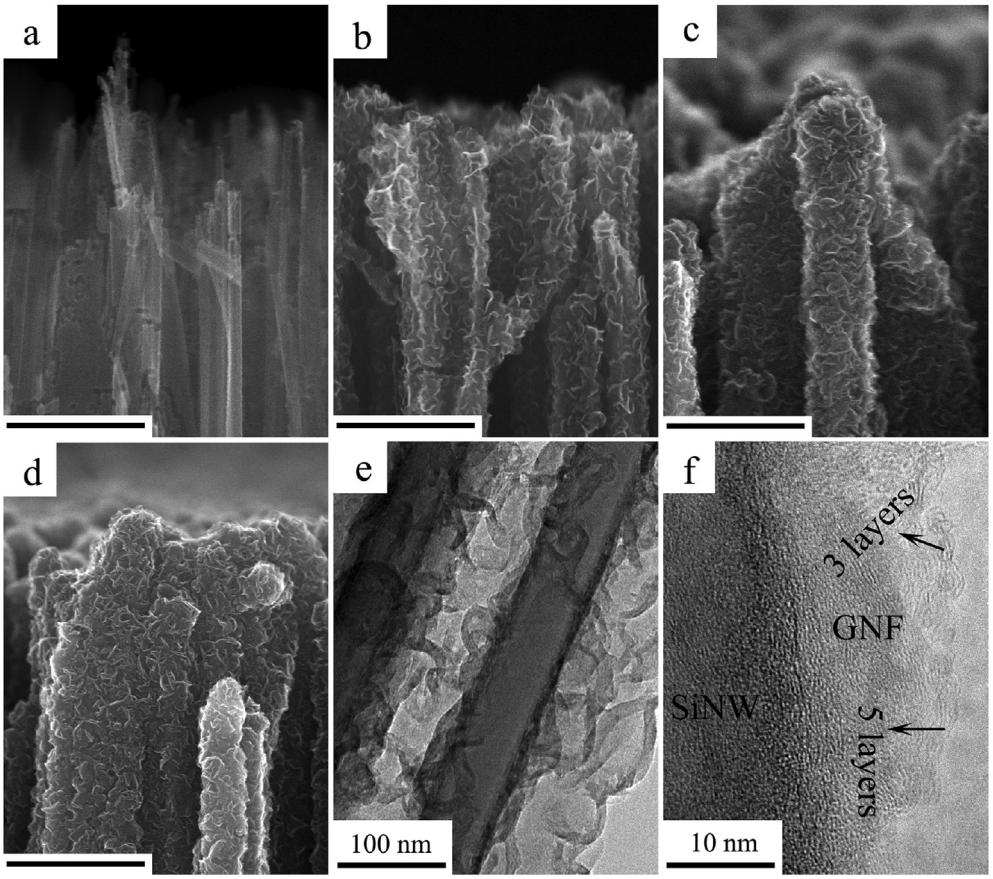

Fig. 8. Side-view SEM images of (a) pristine SiNWs and GNF–SiNW composites synthesized at (b) 4, (c) 5, and (d) 6 sccm C_2H_2. (e) Low- and (f) high-resolution TEM images of the 4 sccm GNF–SiNW composites. Other growth conditions are 1 kPa, 150 W, 800 °C, 10 sccm H_2, and 4 h. The scale bars in (a–d) are 500 nm.

of CNT- and SiNW-based emitters shows that the CNT emitters have far better FE capability. This is ascribed to the better conductivity and higher aspect ratio of CNTs that facilitate electron tunneling through barriers during FE. GNF–SiNW composites with large-sized GNFs were also prepared and their SEM image and FE *J*–*E* curve are shown in Fig. S6a and S6b, respectively. It can be seen that the GNFs are ~1 μm in width and the space among adjacent SiNWs is fully filled by GNFs. For the large-sized GNF sample, the *E* at 1 mA/cm^2 is 5.20 V/μm and the J_{max} is only 1.75 mA/cm^2, both of them are far poorer than those of the small-sized GNF sample (Fig. 8b and Fig. 9a). FE stability of the 4 sccm sample (which has the optimal FE capability) was tested over a period of 15 h, as shown in Fig. 9b. A high J_{mean} of ~1.34 mA/cm^2 is achieved at only 3.450 V/μm and the current fluctuation is negligible. The above results indicate that GNF–SiNW composites with densely distributed and small-sized GNFs and not obviously thickened SiNWs have better FE performance, and these findings are similar as those obtained from the GNF–CNT composites.

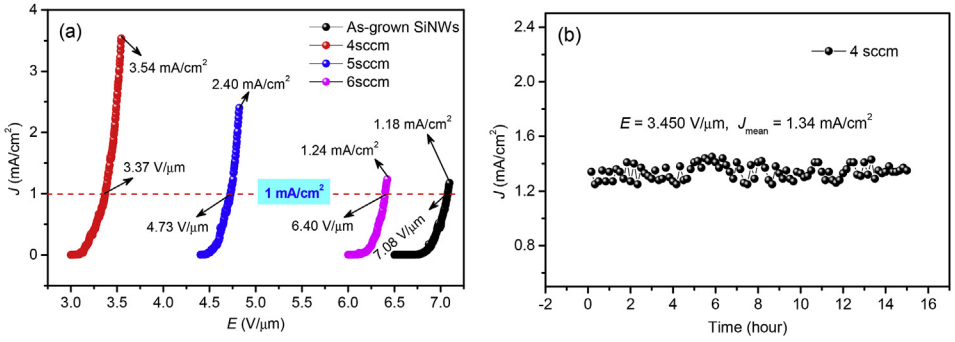

Fig. 9. (a) FE $J-E$ curves of pristine SiNWs and GNF–SiNW composites prepared under 4, 5, and 6 sccm C_2H_2. (b) 15 h FE stability of GNF–SiNW composites prepared under 4 sccm C_2H_2. (A colour version of this figure can be viewed online.)

4. Conclusions

GNFs with different shapes were prepared on CNT and SiNW arrays without a catalyst by using microwave PECVD. The GNFs are vertically aligned on CNTs and SiNWs and have less than 10 layers and are rich in defects. The FE study indicates that GNF–CNT composites with densely distributed and small-sized GNFs and not obviously thickened CNTs have superior FE performance to that of those with sparsely distributed and large-sized GNFs and significantly thickened CNTs. The optimal FE response is obtained from GNF–CNT composites with those optimal shapes. They have a low E_{on} of 0.87 V/μm and E_{th} of 1.54 V/μm and an extremely high J_{max} of 75.46 mA/cm^2, which are far better than 1.20 and 1.77 V/μm and 27.90 mA/cm^2 for the as-grown CNTs, respectively. The small-sized GNFs with nanosharp edges, which serve as highly efficient active emission sites, and the not obviously thickened CNTs, which have high aspect ratios, are both responsible for this improved FE performance. Similar findings are obtained from differently shaped GNF–SiNW composites, *i.e.*, GNF–SiNW composites with densely distributed and small-sized GNFs and not obviously SiNWs have better FE properties. In addition, GNF–CNT composites having the best FE capability are found to also have excellent FE stability at a large J_{mean} of 45.47 mA/cm^2 and a low operation field of 1.766 V/μm over a period of 30 h. Here the GNF–CNT composites with optimal shapes show superior FE properties with low E_{on} and E_{th}, high FE currents, and excellent FE stability under high current densities, which make them good candidates for high-performance vacuum electronic device applications.

Acknowledgments

This work was supported by the National Natural Science Foundation of China for Youth Science Funds (51302187), the Key Project of Tianjin Natural Science Foundation (14JCZDJC32100), and partly by the National Natural Science Foundation of China (51272176). JHD also thanks the financial support from the Tianjin Key Laboratory of Structure and Performance for Functional Molecule and the"131" Innovative Talents cultivation of Tianjin.

Appendix A. Supplementary data

Supplementary data related to this article can be found at http://dx.doi.org/10.1016/j.carbon.2016.02.026.

References

[1] K.S. Novoselov, A.K. Geim, S.V. Morozov, D. Jiang, Y. Zhang, S.V. Dubonos, et al., Electric field effect in atomically thin carbon films, Science 306 (2004) 666–669.
[2] C. Si, W.H. Duan, Z. Liu, F. Liu, Electronic strengthening of graphene by charge doping, Phys. Rev. Lett. 109 (2012) 226802.
[3] K.S. Novoselov, Z. Jiang, Y. Zhang, S.V. Morozov, H.L. Stormer, U. Zeitler, et al., Room–temperature quantum hall effect in graphene, Science 315 (2007) 1379.
[4] S.Y. Zhou, G.H. Gweon, J. Graf, A.V. Fedorov, C.D. Spataru, R.D. Diehl, et al., First direct observation of dirac fermions in graphite, Nat. Phys. 2 (2006) 595–599.
[5] X.W. Ou, L. Jiang, P.L. Chen, M.S. Zhu, W.P. Hu, M.H. Liu, et al., Highly stable graphene-based multilayer films immobilized via covalent bonds and their applications in organic field-effect transistors, Adv. Funct. Mater 23 (2013) 2422–2435.
[6] R.J. Sun, Y. Zhang, K. Li, C. Hui, K. He, X.C. Ma, et al., Tunable photoresponse of epitaxial graphene on SiC, Appl. Phys. Lett. 103 (2013) 013106.
[7] J.L. Yang, J.J. Wang, Y.J. Tang, D.N. Wang, X.F. Li, Y.H. Hu, et al., LiFePO$_4$–graphene as a superior cathode material for rechargeable lithium batteries: impact of stacked graphene and unfolded graphene, Energy Environ. Sci. 6 (2013) 1521–1528.
[8] Z.S. Wu, S.F. Pei, W.C. Ren, D.M. Tang, L.B. Gao, B.L. Liu, et al., Field emission of single-layer graphene films prepared by electrophoretic deposition, Adv. Mater. 21 (2009) 1756–1760.
[9] V. Kaushik, A.K. Shukla, V.D. Vankar, Improved electron field emission from metal grafted graphene composites, Carbon 62 (2013) 337–345.
[10] L.L. Jiang, T.Z. Yang, F. Liu, J. Dong, Z.H. Yao, C.M. Shen, et al., Controlled synthesis of large-scale, uniform, vertically standing graphene for high-performance field emitters, Adv. Mater. 25 (2013) 250–255.
[11] J.L. Du, Y. Zhang, S.Z. Deng, N.S. Xu, Z.M. Xiao, J.C. She, et al., Correlation between topographic structures and local field emission characteristics of graphene-sheet films, Carbon 61 (2013) 507–514.
[12] W.W. Dolan, W.P. Dyke, Temperature-and-field Emission of electrons from metals, Phys. Rev. 95 (1954) 327–332.
[13] W.A. de Heer, A. Châtelain, D. Ugarte, A carbon nanotube field-emission electron source, Science 270 (1995) 1179–1180.
[14] J.H. Deng, X.G. Hou, L. Cheng, F.J. Wang, B. Yu, G.Z. Li, et al., Irradiation damage determined field emission of ion irradiated carbon nanotubes, ACS Appl. Mater. Interfaces 6 (2014) 5137–5143.
[15] S.F. Lee, Y.P. Chang, L.Y. Lee, Synthesis of carbon nanotubes on silicon nanowires by thermal chemical vapor deposition, Carbon 50 (2012) 2061–2064.
[16] X.J. Xu, C.C. Tang, H.B. Zeng, T.Y. Zhai, S.Q. Zhang, H.J. Zhao, et al., Structural transformation, photocatalytic, and field-emission properties of ridged TiO$_2$ nanotubes, ACS Appl. Mater. Interfaces 3 (2011) 1352–1358.
[17] F.H. Chu, C.W. Huang, C.L. Hsin, C.W. Wang, S.Y. Yu, P.H. Yeh, et al., Well-aligned ZnO nanowires with excellent field emission and photocatalytic properties, Nanoscale 4 (2012) 1471–1475.
[18] S.S. Lv, Z.C. Li, C.H. Chen, J.C. Liao, G.J. Wang, M.Y. Li, et al., Enhanced field emission performance of hierarchical ZnO/Si nanotrees with spatially branched heteroassemblies, ACS Appl. Mater. Interfaces 7 (2015) 13564–13568.
[19] H. Sharma, D.C. Agarwal, M. Sharma, A.K. Shukla, D.K. Avasthi, V.D. Vankar, Tailoring of structural and electron emission properties of CNT walls and graphene layers using high-energy irradiation, J. Phys. D. Appl. Phys. 46 (2013) 315301.
[20] Y. Konishi, S. Hokushin, H. Tanaka, L. Pan, S. Akita, Y. Nakayama, Comparison of field emissions from side wall and tip of an individual carbon nanotube, Jpn. J. Appl. Phys. 44 (2005) 1648–1651.
[21] J.O. Hwang, D.H. Lee, J.Y. Kim, T.H. Han, B.H. Kim, M. Park, et al., Vertical ZnO nanowires/graphene hybrids for transparent and flexible field emission, J. Mater. Chem. 21 (2011) 3432–3437.
[22] C.X. Wu, F.S. Li, Y.A. Zhang, T.L. Guo, Improving the field emission of graphene by depositing zinc oxide nanorods on its surface, Carbon 50 (2012) 3622–3626.
[23] R.J. Zou, G.J. He, K.B. Xu, Q. Liu, Z.Y. Zhang, J.Q. Hu, ZnO nanorods on reduced graphene sheets with excellent field emission, gas sensor and photocatalytic properties, J. Mater. Chem. A 1 (2013) 8445–8452.

[24] M. Arif, K. Heo, B.Y. Lee, J. Lee, D.H. Seo, S. Seo, et al., Metallic nanowire–graphene hybrid nanostructures for highly flexible field emission devices, Nanotechnology 22 (2011) 355709.
[25] D.D. Nquyen, N.H. Tai, S.Y. Chen, Y.L. Chueh, Controlled growth of carbon nanotube–graphene hybrid materials for flexible and transparent conductors and electron field emitters, Nanoscale 4 (2012) 632–638.
[26] D.H. Lee, J.A. Lee, W.J. Lee, S.O. Kim, Flexible field emission of nitrogen-doped carbon nanotubes/reduced graphene hybrid films, Small 7 (2011) 95–100.
[27] R.R. Devarapalli, R.V. Kashid, A.B. Deshmukh, P. Sharma, M.R. Das, M.A. More, et al., High efficiency electron field emission from protruded graphene oxide nanosheets supported on sharp silicon nanowires, J. Mater. Chem. C 1 (2013) 5040–5046.
[28] P. Nayak, P.N. Santhosh, S. Ramaprabhu, Enhanced electron field emission of one-dimensional highly protruded graphene wrapped carbon nanotube composites, J. Phys. Chem. C 118 (2014) 5172–5179.
[29] J.L. Liu, B.Q. Zeng, X.R. Wang, W.Z. Wang, H.L. Shi, One-step growth of vertical graphene sheets on carbon nanotubes and their field emission properties, Appl. Phys. Lett. 103 (2013) 053105.
[30] J.H. Deng, R.T. Zheng, Y. Zhao, G.A. Cheng, Vapor-solid growth of few-layer graphene using radio frequency sputtering deposition and its application on field emission, ACS Nano 6 (2012) 3727–3733.
[31] J.H. Deng, G.A. Cheng, Y.M. Yang, R.T. Zheng, Y. Zhao, Excellent field emission characteristics from few-layer graphene/carbon nanotube hybrids synthesized using radio frequency hydrogen plasma sputtering deposition, Carbon 50 (2012) 4732–4737.
[32] K.A. Dean, T.P. Burgin, B.R. Chalamala, Evaporation of carbon nanotubes during electron field emission, Appl. Phys. Lett. 79 (2001) 1873–1875.
[33] S.T. Purcell, P. Vincent, C. Journet, V.T. Binh, Hot nanotubes: stable heating of individual multiwall carbon nanotubes to 2000 K induced by the field-emission current, Phys. Rev. Lett. 88 (2002) 105502.
[34] Y. Wei, K.L. Jiang, L. Liu, Z. Chen, S.S. Fan, Vacuum-breakdown-induced needle-shaped ends of multiwalled carbon nanotube yarns and their field emission applications, Nano Lett. 7 (2007) 3792–3797.
[35] Y.S. Min, E.J. Bae, J.B. Park, U.J. Kim, W. Park, J. Song, et al., ZnO nanoparticle growth on single-walled carbon nanotubes by atomic layer deposition and consequent lifetime elongation of nanotube field emission, Appl. Phys. Lett. 90 (2007) 263104.
[36] C.L. Liu, K.S. Kim, J. Baek, Y. Cho, S. Han, S.W. Kim, et al., Improved field emission properties of double-walled carbon nanotubes decorated with Ru nanoparticles, Carbon 47 (2009) 1158–1164.
[37] S.H. Jo, Y. Tu, Z.P. Huang, D.L. Carnahan, J.Y. Huang, D.Z. Wang, et al., Correlation of field emission and surface microstructure of vertically aligned carbon nanotubes, Appl. Phys. Lett. 84 (2004) 413–415.
[38] A.A. Kuznetzov, S.B. Lee, M. Zhang, R.H. Baughman, A.A. Zakhidov, Electron field emission from transparent multiwalled carbon nanotube sheets for inverted field emission displays, Carbon 48 (2010) 41–46.
[39] J.H. Deng, L. Cheng, F.J. Wang, G.Z. Li, D.J. Li, G.A. Cheng, High current density and longtime stable field electron transfer from large-area densely arrayed graphene nanosheet–carbon nanotube hybrids, ACS Appl. Mater. Interfaces 6 (2014) 21558–21566.
[40] K.Q. Peng, X. Wang, S.T. Lee, Silicon nanowire array photoelectrochemical solar cells, Appl. Phys. Lett. 92 (2008) 163103.
[41] O.A. Louchev, Y. Sato, H. Kanda, Growth mechanism of carbon nanotube forests by chemical vapor deposition, Appl. Phys. Lett. 80 (2002) 2752–2754.
[42] Y.H. Lee, S.G. Kim, D. Tománek, Catalytic growth of single wall carbon nanotubes, Phys. Rev. Lett. 78 (1997) 2393–2396.
[43] M.Y. Zhu, J.J. Wang, B.C. Holloway, R.A. Outlaw, X. Zhao, K. Hou, et al., A mechanism for carbon nanosheet formation, Carbon 45 (2007) 2229–2234.
[44] F. Tuinstra, J.L. Koenig, Raman spectrum of graphite, J. Chem. Phys. 53 (1970) 1126–1130.
[45] R.J. Nemanich, S.A. Solin, First- and second-order raman scattering from finite-size crystals of graphite, Phys. Rev. B 20 (1979) 392–401.
[46] A.C. Ferrari, J.C. Meyer, V. Scardaci, C. Casiraghi, M. Lazzeri, F. Mauri, et al., Raman spectrum of graphene and graphene layers, Phys. Rev. Lett. 97 (2006) 187401.
[47] F.J. Wang, L.N. Deng, J.H. Deng, Facile synthesis of differently shaped, ultrathin, and aligned graphene flakes without a catalyst for highly efficient field emission, Appl. Surf. Sci. 355 (2015) 218–225.
[48] I.J. Teng, C.S. Huang, H.L. Hsu, I.C. Chung, S.R. Jian, N.P. Kherani, et al., On the use of new oxidized Co–Cr–Pt–O catalysts for vertically-aligned few-walled carbon nanotube forest synthesis in electron cyclotron resonance chemical vapor deposition, Carbon 80 (2014) 808–822.
[49] Y. Zhang, J.L. Du, S. Tang, P. Liu, S.Z. Deng, J. Chen, et al., Optimize the field emission character of a vertical few-layer graphene sheet by manipulating the morphology, Nanotechnology 23 (2012) 015202.
[50] R.H. Fowler, L. Nordheim, Electron emission in intense electric fields, Proc. R. Soc. Lond. Ser. A 119 (1928) 173–181.
[51] G. Kim, B.W. Jeong, J. Ihm, Deep levels in the band gap of the carbon nanotube with vacancy-related defects, Appl. Phys. Lett. 88 (2006) 193107.
[52] L.B. Zhu, Y.Y. Sun, D.W. Hess, C.P. Wong, Well-aligned open-ended carbon nanotube Architectures: an approach for device assembly, Nano Lett. 6 (2006) 243–247.
[53] J.H. Deng, L. Cheng, F.J. Wang, B. Yu, G.Z. Li, D.J. Li, et al., Ultralow field emission from thinned, open-ended, and defected carbon nanotubes by using microwave hydrogen plasma processing, Appl. Surf. Sci. 324 (2015) 293–299.
[54] Y.F. Guo, W.L. Guo, Electronic and field emission properties of wrinkled graphene, J. Phys. Chem. C 117 (2013) 692–696.
[55] G. Wei, Emission property of carbon nanotube with defects, Appl. Phys. Lett. 89 (2006) 143111.
[56] M. Araidai, Y. Nakamura, K. Watanabe, Field emission mechanisms of graphitic nanostructures, Phys. Rev. B 70 (2004) 245410.
[57] J.C. She, N.S. Xu, S.Z. Deng, J. Chen, H. Bishop, S.E. Huq, et al., Vacuum breakdown of carbon-nanotube field emitters on a silicon tip, Appl. Phys. Lett. 83 (2003) 2671–2673.
[58] H.S. Jang, S.K. Jeon, S.H. Nahm, Field emission properties from the tip and side of multi-walled carbon nanotube yarns, Carbon 48 (2010) 4019–4023.
[59] Y. Saito, K. Hamaguchi, S. Uemura, K. Uchida, Y. Tasaka, F. Ikazaki, et al., Field emission from multi-walled carbon nanotubes and its application to electron tubes, Appl. Phys. A 67 (1998) 95–100.
[60] H.J. Jeong, H.D. Jeong, H.Y. Kim, J.S. Kim, S.Y. Jeong, J.T. Han, et al., All-carbon nanotube-based flexible field-emission devices: From cathode to anode, Adv. Funct. Mater. 21 (2011) 1526–1532.
[61] J.S. Suh, K.S. Jeong, J.S. Lee, I. Han, Study of the field-screening effect of highly ordered carbon nanotube arrays, Appl. Phys. Lett. 80 (2002) 2392–2394.
[62] Y.J. Hung, S.L. Lee, L.C. Beng, H.C. Chang, Y.J. Huang, K.Y. Lee, et al., Relaxing the electrostatic screening effect by patterning vertically-aligned silicon nanowire arrays, Thin Solid Films 556 (2014) 146–154.